ARMY RESEARCH LABORATORY

Experimental Results of an Electrostatic Injector

by M Ryan, J Tennis, D Eichner, Z Lee, T Sowell, M Benson, B Van Poppel, MS Kurman, and C-B M Kweon

ARL-RP-0507 **October 2014**

Reprinted from ILASS-Americas [accessed 2014 Oct 9]. http://www.ilass.org/2/conferencepapers/38_2014.pdf. Paper presented at: AIAA ILASS Americas 26th Annual Conference on Liquid Atomization and Spray Systems; 2014 May; Portland, OR.

NOTICES

Disclaimers

The findings in this report are not to be construed as an official Department of the Army position unless so designated by other authorized documents.

Citation of manufacturer's or trade names does not constitute an official endorsement or approval of the use thereof.

Destroy this report when it is no longer needed. Do not return it to the originator.

Army Research Laboratory
Aberdeen Proving Ground, MD 21005-5066

ARL-RP-0507 **October 2014**

Experimental Results of an Electrostatic Injector

M Ryan, J Tennis, D Eichner, Z Lee, T Sowell, M Benson, and B Van Poppel
United States Military Academy

MS Kurman and C-B M Kweon
Vehicle Technology Directorate, ARL

Reprinted from ILASS-Americas [accessed 2014 Oct 9]. http://www.ilass.org/2/conferencepapers/38_2014.pdf. Paper presented at: AIAA ILASS Americas 26th Annual Conference on Liquid Atomization and Spray Systems; 2014 May; Portland, OR.

REPORT DOCUMENTATION PAGE

Form Approved
OMB No. 0704-0188

1. REPORT DATE *(DD-MM-YYYY)*	2. REPORT TYPE	3. DATES COVERED (From - To)
October 2014	Reprint	October 2013–March 2014

4. TITLE AND SUBTITLE
Experimental Results of an Electrostatic Injector

5a. CONTRACT NUMBER

5b. GRANT NUMBER

5c. PROGRAM ELEMENT NUMBER

6. AUTHOR(S)
M Ryan, J Tennis, D Eichner, Z Lee, T Sowell, M Benson, B Van Poppel, MS Kurman, and C-B M Kweon

5d. PROJECT NUMBER

5e. TASK NUMBER

5f. WORK UNIT NUMBER

7. PERFORMING ORGANIZATION NAME(S) AND ADDRESS(ES)
U.S. Army Research Laboratory
ATTN: RDRL-VTP
Aberdeen Proving Ground, MD 21005-5066

8. PERFORMING ORGANIZATION REPORT NUMBER
ARL-RP-0507

9. SPONSORING/MONITORING AGENCY NAME(S) AND ADDRESS(ES)

10. SPONSOR/MONITOR'S ACRONYM(S)

11. SPONSOR/MONITOR'S REPORT NUMBER(S)

12. DISTRIBUTION/AVAILABILITY STATEMENT
Approved for public release; distribution is unlimited.

13. SUPPLEMENTARY NOTES
Reprinted from ILASS-Americas [accessed 2014 Oct 9]. http://www.ilass.org/2/conferencepapers/38_2014.pdf.
Paper presented at: AIAA ILASS Americas 26th Annual Conference on Liquid Atomization and Spray Systems; 2014 May; Portland, OR.

14. ABSTRACT
The objective of the current research is to assess the effects of electrostatic injector designs and charge energy on the spray break-up process of JP-8 fuel. Electrostatic injectors improve the liquid fuel spray atomization at low fuel pressures through the introduction of additional columbic forces on the spray particles. While charge injection introduces the columbic forces on the fuel before the nozzle exit, electrostatic injection applies the electric potential to the spray immediately after the fuel exits the nozzle. The application areas include carbureted and port fuel injections in small engines to improve fuel-air mixing. In this study, two different electrostatic injector designs were tested in an ambient chamber with four optical windows. The separate designs consist of basic slot nozzle geometries with varying nozzle dimensions as well as different electrode setups. Shadowgraphy and Mie scattering techniques were used to assess the spray characteristics such as spray patterns, onset of break-up, and atomization. Shadowgraphy with a micro zoom lens was used to measure droplet distributions and droplet velocities. The tests, which were conducted at the ARL Spray Combustion Research Laboratory in Aberdeen Proving Ground, MD, consist of a constant JP-8 spray and a single 7 ms electric potential pulse of up to 3 kV. The quantitative and qualitative analysis of the results is presented to characterize the behavior of electrostatic injector designs. Both of the electrostatic injectors analyzed in this study were able to produce break-up in the fuel spray at various Reynolds numbers and applied electrostatic charges.

15. SUBJECT TERMS
fuel injector, JP-8, electrostatic, spray breakup

16. SECURITY CLASSIFICATION OF:			17. LIMITATION OF ABSTRACT	18. NUMBER OF PAGES	19a. NAME OF RESPONSIBLE PERSON
a. REPORT	b. ABSTRACT	c. THIS PAGE			M Ryan
Unclassified	Unclassified	Unclassified	UU	16	19b. TELEPHONE NUMBER (*Include area code*) 410-278-9319

Standard Form 298 (Rev. 8/98)
Prescribed by ANSI Std. Z39.18

Experimental Results of an Electrostatic Injector

M. Ryan*, J. Tennis, D. Eichner, Z. Lee, T. Sowell, M. Benson, and B. Van Poppel
Department of Civil & Mechanical Engineering
United States Military Academy
West Point, NY, USA

M. S. Kurman, C-B. M. Kweon
U.S. Army Research Laboratory
Aberdeen Proving Ground, MD, USA

Abstract

The objective of the current research is to assess the effects of electrostatic injector designs and charge energy on the spray break-up process of JP-8 fuel. Electrostatic injectors improve the liquid fuel spray atomization at low fuel pressures through the introduction of additional columbic forces on the spray particles. While charge injection introduces the columbic forces on the fuel before the nozzle exit, electrostatic injection applies the electric potential to the spray immediately after the fuel exits the nozzle. The application areas include carbureted and port fuel injections in small engines to improve fuel-air mixing. In this study, two different electrostatic injector designs were tested in an ambient chamber with four optical windows. The separate designs consist of basic slot nozzle geometries with varying nozzle dimensions as well as different electrode setups. Shadowgraphy and Mie scattering techniques were used to assess the spray characteristics such as spray patterns, onset of break-up, and atomization. Shadowgraphy with a micro zoom lens was used to measure droplet distributions and droplet velocities. The tests, which were conducted at the ARL Spray Combustion Research Laboratory in Aberdeen Proving Ground, MD, consist of a constant JP-8 spray and a single 7 ms electric potential pulse of up to 3 kV. The quantitative and qualitative analysis of the results is presented to characterize the behavior of electrostatic injector designs. Both of the electrostatic injectors analyzed in this study were able to produce break-up in the fuel spray at various Reynolds numbers and applied electrostatic charges.

*Corresponding author: matthew.ryan2@usma.edu

Introduction

The objective of this research is to assess the effects of electrostatic injector design and charge energy on the spray break-up process. Electrostatic injectors have the potential to improve the liquid fuel spray break-up at low fuel pressures. The application areas include carbureted and port fuel injections in small engines to improve fuel-air mixing. Based on TDA Research and University of Colorado study of electrostatic injectors, this research looks at electrostatic injector spray in an ambient chamber with four optical windows [1]. Shadowgraphy with a micro zoom lens was used to qualitatively analyze the spray. The experiments in this project consist of baseline tests on an electrostatic injector designed by TDA Research Inc. followed by additional tests with similar parameters on an injector designed by the United States Military Academy Department of Civil and Mechanical Engineering. The analysis provides insights into the electrostatic charging effect on spray break-up from the baseline tests as well as comparisons with the results of the USMA injector.

Background

Charged spray configurations have been investigated since Lord Rayleigh's work near the turn of the last century. Rayleigh established what would become the field of electrohydrodynamics, demonstrating the dynamics of a liquid drop in an electric field [3]. G.I. Taylor investigated liquid dispersion through a capillary tube. His description of the behavior of electrically-driven liquids would become known as the Taylor Cone [2, 4]. Kim and Turnbull were responsible for the progression of electrohydrodynamic methods to enhance atomization in the context of combustion applications [5]. They used a needlelike electrode with a high voltage potential to induce a charge in a flowing liquid [5]. Shrimpton and Yule used a similar technique in their "Spray Triode" [6]. As shown in Figure 1, the spray triode first consists of the nozzle, which is generally a hollow cone shape but could also be constructed in a flat fan configuration. Inserted into the nozzle is the high-voltage electrode. This electrode induces a charge on the fuel before it leaves the nozzle exit plane. The spray triode has proven successful in injecting charge into liquids with a low electrical conductivity without the requirement of any additives [7, 8]. Generally, higher voltages result in an increasing number of droplets with smaller average diameters until a threshold is reached with the fuel, and the effect rapidly diminishes. Three ideas attempt to explain this phenomenon, including the concept of electron emission, field ionization, and coronal discharge [8].

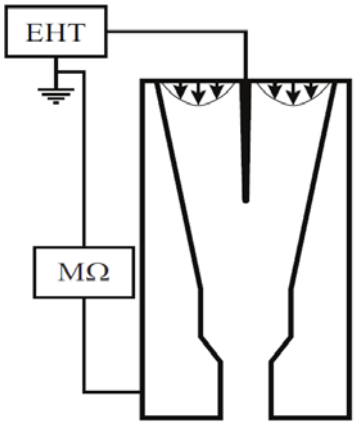

Figure 1. Spray triode [6]

Shrimpton conducted further work with charge injections by comparing dielectric and semi-conducting liquids within the Spray Triode. The atomization of dielectric liquids improved with increasing flow rate. Shrimpton's work also showed the benefits of electrostatic charge on fuel injectors as he more finely atomized the fuel, which resulted in increased combustion efficiently for these dielectric liquids [10].

Recently, electrostatic injectors have shown potential to improve liquid fuel spray break-up at much lower fuel pressures, which is important especially in the realm of biofuels. In the long term, the United States Department of Defense (DOD) is interested in converting many of their vehicles to biofuels. Both the U.S. Army and Navy have invested substantially into research pertaining to converting existing fleets to biofuel compatibility. The recent work of Owkes and Desjardins has investigated the effects of electrostatic spray with biofuels [11]. They utilized computational fluid dynamics (CFD) to model the spray dynamics of biofuels. Their results show electrostatic charge can also have a substantial influence on the injection behavior of biofuels.

Electrostatic Injection

There are three methods for inducing charge in the electrohydrodynamic field. The two previously discussed are Shrimpton's direct charge injection and Rayleigh's colloid propulsion. The third technique induces charge on a liquid by spraying it through an electric field downstream of the nozzle. This external charge concept is already utilized in other application areas such as fine spray painting. The idea is to pass the liquid sheet through an electric field to induce charge on the fluid as shown in Figure 2. In TDA Research's initial study and this study, a downstream charge induction is utilized [1].

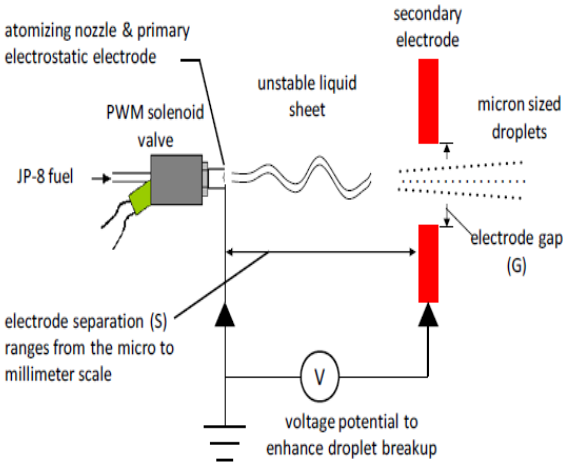

Figure 2. Downstream charge induction [1]

In downstream charge induction, the liquid is sprayed out through a typical nozzle and then passed between two electrodes. One electrode has an applied voltage while the other is attached to the ground and acts as the return for the current. The gap between the electrodes creates an electric field. As the liquid molecules pass through the electric field, a charge is induced on the molecules. Like charges cause the molecules to repel initiating earlier break-up and increased atomization. Increasing the voltage for both TDA Research's and Shrimpton's direct charge injection nozzles show increased levels of atomization. This behavior continues to a finite voltage level at which no further atomization improvements can be observed. The threshold is achieved when the charge density of the fuel is maximized. For higher voltages, the charge density and resulting atomization decreases significantly with the occurrence of coronal discharge [7, 8].

Test Fuel: JP-8

Since the 1980s the U.S. Military has sought to utilize a single fuel for all its vehicles [12]. This would greatly reduce logistical costs. In accordance with DOD's "Single Fuel Forward" the U.S. Army is investigating the development of low pressure JP-8 injected engines for unmanned aerial systems [12]. Per Army requirements associated with transport and safety, (MIL-DTL-83133H), JP-8 must have additives which increase the conductivity of the fuel [13]. In its natural form JP-8 is a hydrocarbon with extremely low conductivity. Shearing forces present in fuel flow lines cause charge separation and increased levels of electrostatic charge. With fuels this can become dangerous in the presence of static discharges. As a result, the military specification requires additives that increase electric conductivity to disperse and relax the electrostatic charge [13]. As a result, JP-8 is particularly suited for electrostatic application because of this increased electrical conductivity. Callister and Rethwisch define electrical conductivity as the ease at which a material is capable of conducting current [14]. An increase in electrical conductivity increases the ability to induce charge on the fuel. However, the increased conductivity also includes a decrease in the dielectric force, and an increase in surface effects due to nearly instantaneous charge relaxation.

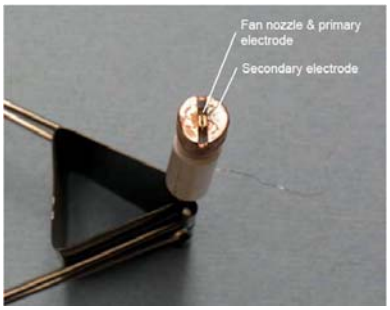

Figure 3. Flat fan injector [1]

USMA Injector Design

A substantial difference was implemented to improve upon the behavior of the injector used in [1] and the design reported herein, which is referred to as the USMA injector. TDA Research used a nozzle with a flat fan configuration while the existing design consisted of a rectangular slot. Additionally, TDA Research injector's streamwise length served as the ground electrode while the cap acted as the positive electrode; the present injector sets both electrodes at the exit of the nozzle. Instead of the solid cap used by TDA Research, the revised cap was split into half in order to allow additional build-up of charge on one side of the nozzle exit, perpendicular to the breadth of the rectangular fuel stream. As the following description of the fabrication explains, one challenge with the present design includes insulating the two electrodes from each other as well as from the nozzle itself.

The USMA injector consists of four pieces, one of which is divided into two sub-components. The design includes an electrode cuff, which connected to the high voltage source and the ground, the injector nozzle with a slot orifice, a Teflon spacer to insulate the injector nozzle from the high voltage, and an injector tube to connect the nozzle to the metered test bench outlet. The electrode cuff, injector nozzle and injector tube were all made out of Copper Alloy 145 to enhance conductivity. The cuff, spacer, and tube were locally fabricated. The injector nozzle was outsourced to an EDM laboratory due to the relatively small scale of the orifice. Since future simulations will rely on the actual nozzle geometry, the techniques used to manufacture and assemble are presented in the following sections.

Electrode Cuff

The electrode cuff was fabricated as two distinct pieces to ease manufacturing, and then joined. The first piece included the base of the cuff and the inner collar. This consisted of several sharp angles and precise cuts on the lathe.

To produce this part, a custom lathe tool was made out of high carbon steel utilizing a precision mill. This lathe tool consisted of sharp corners with a radius of curvature on the order of 0.001" and 79° corners to ensure only the corner of the tool removed material.

The first part of the electrode cuff was made by turning down a 0.5" copper rod that was 2.0" in length. The center was first drilled out to a diameter slightly smaller than the inner diameter of the inside collar. A 5/32" drill bit was used to hollow out the inside of the rod and the remaining 0.006" was removed using the lathe tool for an inner diameter of 0.162". Next the lathe tool was used to shave down the rod to the diameter of the cuff base which was 0.300". A shoulder in the part was then made where the second cuff component would slide on. This meant taking the diameter of the rod down to 0.250" at a length of 0.015". Finally, to create the inner collar, the rod was turned down to an outer diameter of 0.188". Figure 4 shows this component design.

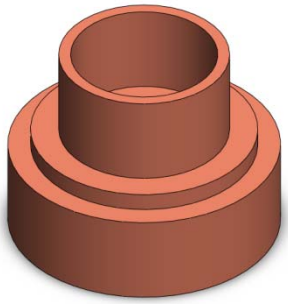

Figure 4. Sub-component of the electrode cuff

The second part of the electrode cuff is the outer collar. This consisted of a simple ring with an outer and inner diameter of 0.300" and 0.250" respectively. This collar was 0.215" in length and turned down from a 0.500" copper rod on a lathe.

To join the two sub-components, the first part was placed in a collet so that it was straight. A ring of solder was placed around the shoulder that was turned down. The outer collar was then placed onto the solder in the shoulder and the joint was heated with a butane torch. The electrode cuff was only heated to the melting point of the solder briefly indicating the two parts were joined. This created a bind capable of transferring the high electric potential in addition to providing a smooth and seamless bond.

The joined pieces were transferred to a block collet and placed in the mill. The mill was fitted with a 0.008" slitting saw in order to produce the 0.045" gap between cuffs. At a speed of 550 rpm, six passes were used to produce the correctly sized gap. The final step was to face the base of the cuff on the lathe for a smooth finish so it did not interfere with the spray. The joined design is depicted in Figure 5.

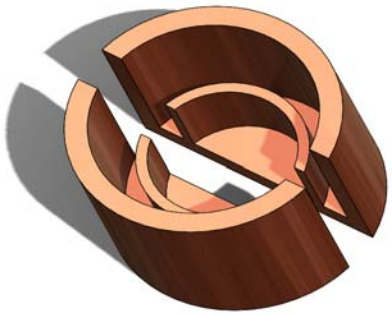

Figure 5. Electrode cuff design

Teflon Spacer and Injector Tube

These two components of the spray nozzle were the easiest to manufacture as their shape was more basic than the electrode cuff. The Teflon began as a solid rod and was turned down to an outer and inner diameter to match the spacing between the inner and outer collars of the electrode cuff. The inner diameter also matched the outer diameter of the injector nozzle which was 0.188" so the injector could slip inside. The injector tube started as a copper tube with a nominal outer diameter of 0.125". The outside was turned down to a diameter of 0.124" so that it could be fitted inside the injector nozzle which has an inner diameter of 0.123". Both the Teflon spacer and injector tube were fabricated on a lathe.

Injector Nozzle

In order to have the injector nozzle manufactured, it had to be outsourced to an electrical discharge machining (EDM) company. This design was sent to EDM Laboratories, Inc. in Corpus Christi, Texas. This company was selected based upon their ability to auto thread wire as small as 0.004" in diameter. This small of a wire was critical to the fabrication of this nozzle since the orifice dimensions were 0.031" x 0.008". EDM Laboratories system is mounted on a radial drill that can articulate in five axes. This allowed them to create the smooth entrance into the orifice inside the nozzle. The final nozzle design is shown in Figure 6, highlighting the orifice and the smooth entrance.

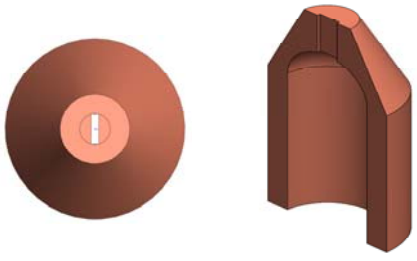

Figure 6. Injector nozzle

Assembly

Most of the USMA injector parts were assembled using compression fittings based on the tight tolerances that the components were built to. The Teflon spacer was fitted over the injector nozzle until the top of the spacer lined up with the top of the nozzle. Next, the two cuffs were pressed into the spacer. The two collars hugged onto the spacer to prevent them from falling off. The only non-compression fitting was the nozzle onto the tube. The end of the injector rod was turned down to slip into the nozzle and lightly covered with solder. When the tip of the rod was slipped into the nozzle, the solder was sealed with the propane. In addition to providing a connection, the solder sealed the nozzle to the injector which prevented the fuel from leaking. The final dimensions of the assembly are an orifice of 200 x 780 µm and the electrode cuff gap was 1150 µm. Figure 7 shows the final assembly of all the components once manufacturing was complete.

Figure 7. Actual USMA injector assembly

Test Methods

The experimental setup for this investigation was a two step process. The first was the design and construction of a fuel bench for the testing protocol. TDA Research's slot electrostatic injector was utilized with varying charge voltage and fuel pressures to obtain shadowgraph images of different sprays and qualitatively compare results under differening spray conditions. Next, a unique electrostatic injector was designed and similar tests were conducted using the same experimental setup.

Test Bench Design

The fuel bench design focused on maximizing the controlled conditions of the flow and electrostatic charges, including pressure, temperature, voltage, pulse widths, and frequency. Figure 8 shows a schematic of the design.

Fuel delivery is achieved by an Aeromotive 11101 pump that passes the liquid through two fuel filters at 100 µm and 10 µm. The fuel then flows through an accumulator and a cross-flow heat exchanger. The heat exchanger is controlled by an Omega temperature controller with chilled water as the coolant. The fuel proceeds through a pressure regulator and fast response solenoid valve where it can be pulsed into the injector. The fuel is sprayed into a custom-designed plexiglas spray chamber. The chamber has transparent windows to ensure the highest quality shadowgraph images.

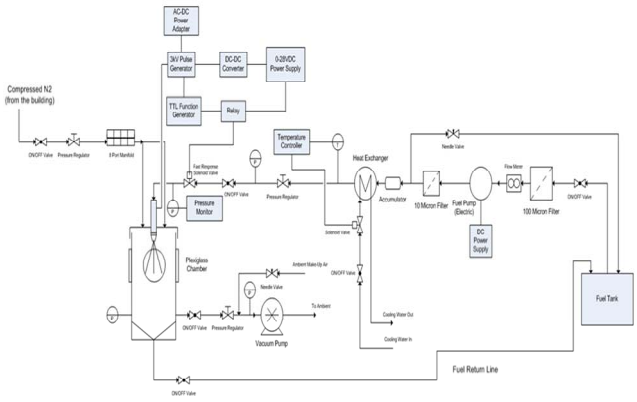

Figure 8. Schematic of experimental setup

The electrical system is equally important for electrostatic injectors. Figure 9 shows an enlarged version of the electric system in the test bench.

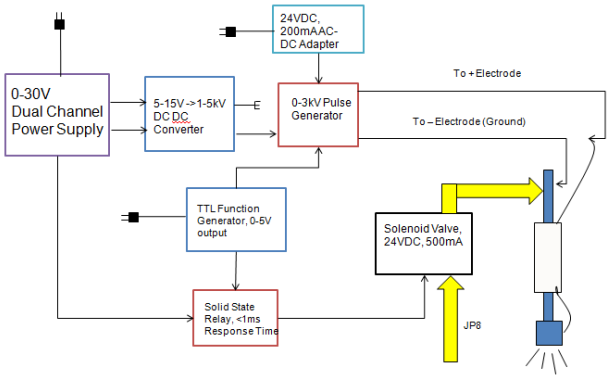

Figure 9. Schematic of electric system

The power supply for the components of Figure 9 comes from the dual channel 0-30 V power supply. The voltage is stepped up in a DC-DC converter with an output capacity of 15 kV. The voltage is then pulsed in a pulse generator, which in turn is controlled by a TTL function generator. That same function generator controls a solid state relay which pulses the fuel.

Experimental Procedures

The baseline tests goals were to reproduce TDA Research's initial results, including the evidence of increased atomization due to the electrostatic charge. In order to visually investigate shadowgraphy tests were completed. Shadowgraphy uses a light source shining directly towards the camera through the spray to transmit the spray's shadow on the camera. Shadowgraphy is particularly useful with flat fan nozzles because of the small thickness and predominantly two dimensional nature of the spray. A Photron SA5 Fastcam camera was scaled and focused for the imaging using a plate with two dots at known separation distance. These dots were maintained in the viewing area of the camera and set a coordinate origin using

LaVision's DaVis software, so that proper length scales could be established in both directions.

To simplify the timing of the fuel spray, the applied voltage, and the acquisition by the camera system, a constant fuel spray was employed. A Stanford Research Systems DG645 Digital Delay Generator was used to initiate the applied voltage and trigger the camera. Images with and without an applied electrostatic charge were recorded by using a 1 ms delay from the start of the camera acquisition prior to the voltage trigger. Through iteration with the high voltage digital multimeter, it was determined the voltage would required a pulse width of 5 ms to properly build up on the injector cap, so a 6 ms pulse width was used. The camera recorded a total of 20 ms allowing the analysis of both the voltage build up and draw down. Images were captured with 1 μs exposure time and recorded at 40,000 frames/sec (fps). This exposure time is important because the fuel spray was maintained at relatively low pressure and spray velocities; as such it can be concluded that each frame captures an instantaneous image. Figure 10 shows the camera set up at the spray chamber.

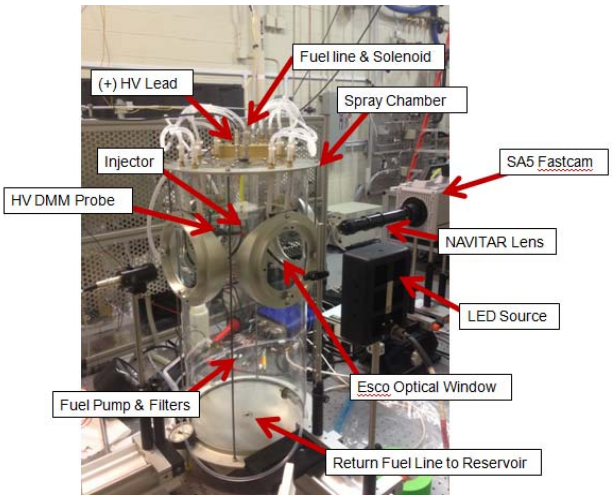

Figure 10. Experimental setup

After the voltage was applied, the fuel temperature was measured with a Type-K thermocouple wired to an Omega i-series temperature controller. The fuel pressure was measured with a pressure transducer and an Omega i-series pressure monitor. The voltage potential at the injector was measured with the high-voltage digital multimeter. The method to calculate the uncertainty associated with the Reynolds and Weber numbers for the experiment utilizes the technique for multi-sample uncertainty described by Kline-McClintock [19].

Experimental Conditions

The first experimental conditions were based on TDA Research's previous work and used a similar nozzle to the one in their report [1]. Fuel was sprayed at various conditions outlined in Table 1 including a range of voltage potentials in 500 V increments.

Table 1. Experimental conditions for the TDA Research injector

Pressures (psi)	Reynolds Number	Weber Number
2	780	110
4	1090	210
6	1550	440
8	2180	860

Voltages (V)
0
500
1000
1500
2000
2500
3000

Images were collected at the nozzle exit region and in the break-up region of the flows.

The tests conducted on the injector varied pressures from 2 to 25 psi in order to observe the effects of the electrostatic injection beyond the capabilities of the TDA Research injector. Of note, the rectangular orifice of the USMA injector produced more steady streams than the TDA Research flat fan orifice which allowed for testing at higher pressures without obstruction challenges.

Processing Methods

LaVision's Data Acquisition and VISualization (DAVIS) Software (Version 8) was utilized to analyze the shadowgraphy videos. Efforts were made to minimize the effect of variations in background light distribution by defining a filter radius kernel of approximately 1.5 times the typical particle diameter in the set. Local definitions of the light intensity were utilized to identify liquid droplets across the range of pixels within an interrogation window. This intensity threshold varied between videos with significantly different spray structures or camera position. The definition of a particle within a range of intensities was set according to these intensity levels. A particle size filter was applied to most of the files to prevent the software from defining large non-uniformly sized liquid regions and ligaments as individual droplets. In this analysis there exists a natural trade-off between particle identification and the relative noise level, so care was taken to be conservative in the threshold levels used.

Results using the TDA Research Injector

The first set of results depicted in Figure 11 represents the TDA Research injector tested at similar conditions to that study [1]. Because of substantive difference in the flow setup and documentation, a direct comparison was not the goal of these tests. Instead, the general behavior of increased atomization due to the presence of an increasing electrostatic charge was sought.

Figure 11 is organized vertically by applied voltage and horizontally by Reynolds and Weber numbers. All the images were taken at the same time step of 8 ms. At 8 ms the applied voltage is discontinued, and the effects of the electric field are clearly visible. Readily apparent is that

there is increased atomization as the voltage potential is increased. Moving from left to right the surface tension effects are more noticeable as the Reynolds number increases. The rims and ligaments in the spray during the onset of atomization illustrate these surface tension effects.

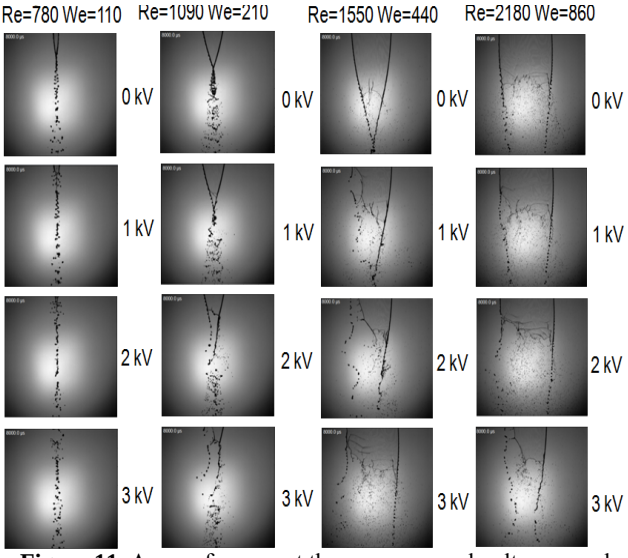

Figure 11. Array of sprays at the pressures and voltages used by TDA Research.

Figure 12 shows a sample of images at the uncharged (left) and charged (right) condition when Re=780 and We=110. The images each include the nozzle exit plane and extend 37 nozzle diameters downstream, and pre and post images support the claim that the images can be considered instantaneous. There is no visible breakup of the uncharged spray with clearly defined rims and a relatively symmetric spray sheet. The right image is taken at 14350 µs after the camera was triggered. This image displays spray with a 3.14 kV induced electrical potential, and indicates the effects in terms of the onset of atomization and the instability of the disturbed rims at the edge of the liquid sheet. The break-up effects from the electrical charge were present in the spray even though the charge was discontinued after 8 ms. The extended response is attributed to the time necessary for the spray to return to its uncharged state.

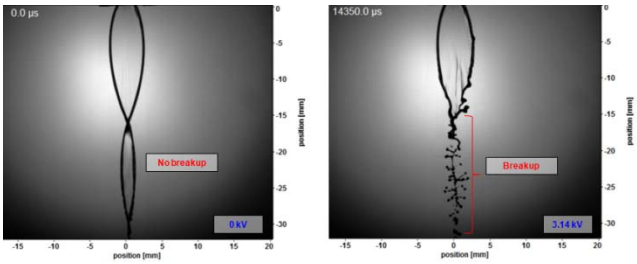

Figure 12. Re=780 We=110

Figure 13 is similar to Figure 12 in that the photo is taken at the nozzle, the applied voltage is 3 kV, and enhanced breakup can be seen in the charged condition. Figure 13 does introduce a concept not seen in Figure 12. The break-up region in Figure 13 has increased ligamentation due to the higher pressure condition at which they were obtained, with evidence of the surface tension effects apparent for the liquid sheet furthest from the nozzle exit.

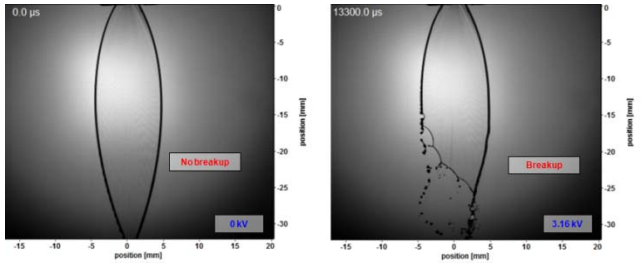

Figure 13. Re=1090 We=210

Figure 14 depicts another increase in Reynolds and Weber numbers. Figure 14 also shows the liquid sheet break up closer to nozzle with the voltage applied despite the increased momentum of the liquid phase. Edge effects are also evident in the charged case, and the ligaments show small scale ripples in the spanwise direction. Figure 14 also highlights an increased asymmetry of the spray. Possible explanations include fabrication or surface roughness effects for the nozzle geometry, or an uneven distribution of the electrical charge.

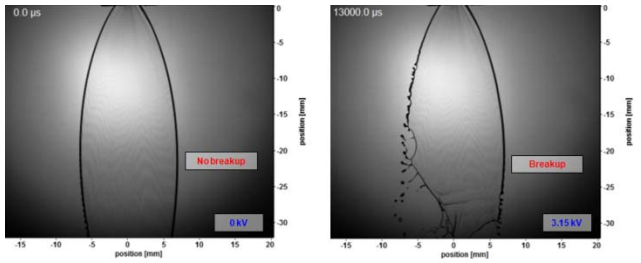

Figure 14. Re=1550 We=440

In Figure 15 the camera is focused 40.6 nozzle diameters down from the nozzle exit to focus on the break up region. In Figure 15 the horizontal spread of the droplets when the voltage is applied in increased. Individual droplets are visible up to 17 nozzle diameters away from the image center.

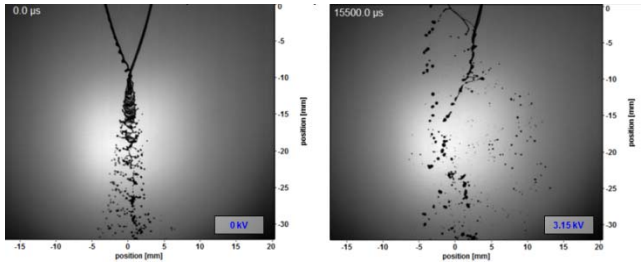

Figure 15. Re=1090 We=210

Figure 16 shifts downstream to a position 42.6 diameters from the nozzle exit plane. With a Reynolds number of 1550, Figure 16 is the best to examine the edge effects of the spray between the charged and uncharged cases. Ligaments and ripples are clearly enhanced when voltage is applied. While the break up region is evident in each case, the charged condition shows broader dispersion in both dimensions.

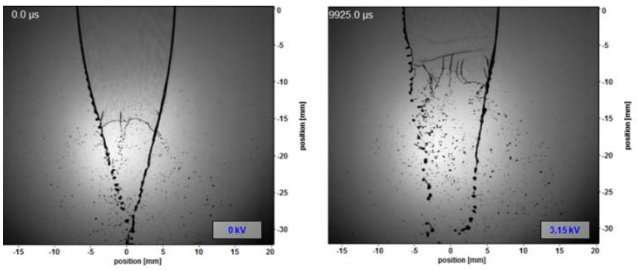

Figure 16. Re=1550 We=440

The next set of analyses for the TDA Research injector utilized time averaged sets of images focused on the breakup region. The effects of the sprays at four Reynolds numbers and two different voltages, 2 kV and 3 kV, are discussed for a 25 ms time record along with the corresponding uncharged case. For the charged cases, a 6 ms pulse width was applied with records initiated 1 ms prior to the charge application.

Figure 17 displays the droplet distribution for the range of charged cases described. The horizontal axis displays the range of observed droplet sizes for each spray while the vertical axis aggregates the total number of particles at each size.

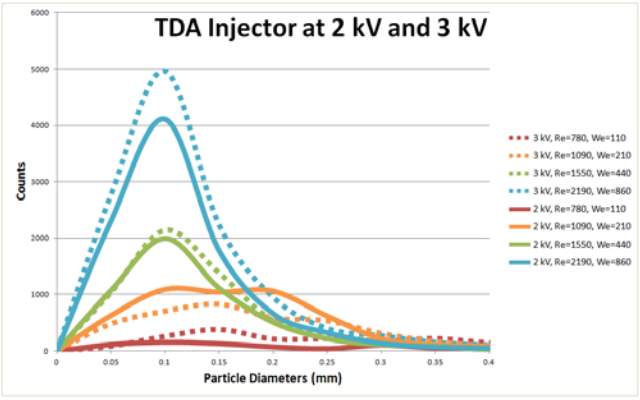

Figure 17. Droplet distributions for various Reynolds and Weber numbers and at two applied voltages.

The distribution at a Reynolds number of 780 appears to have a wide range of droplet distributions. The wide range of droplet sizes is a result of a lower Reynolds number and the described processing method. The LaVision software has difficulty in discerning between droplets, ligaments, as well as light diffractions in the sheet of the spray. However, as the Reynolds number increases the quality of the droplet distribution improves. The clearest distributions are at a Reynolds number of 1550, characterized by the largest peaks, and display the expected distribution of an atomized spray. Most particles are in the 0.01-0.15 mm range with over 4000 droplets below 0.1 mm diameter.

Compared to the 2 kV sets, the droplet distribution at the same Reynolds numbers for each condition is larger in overall number of particles and smaller in the droplet diameters for the 3 kV sets. The same Reynolds number conditions at the different applied voltages generally resemble each other in the shape of the droplet distribution. The only inconsistency with the expected results of these TDA injector distributions occurs with the different voltage sets at a Reynolds number of 1090. In this case, the 2 kV distribution contains more droplet particles than its 3 kV counterpart.

While the plots of the droplet distribution provide insight into the nature of each spray, the data in Table 2 are the defining characteristics of the 2 kV sprays. The total number of particles observed in the videos increases with the higher pressure. Included in this data is the mean diameter, D10, and the Sauter Mean Diameter, D32, which both decrease as the Reynolds number increases. Also, the maximum droplet diameter is provided for a cumulative droplet volume of 10%, 50%, and 90%. These behave as expected with the exception of DV50 and DV90 for the two lowest Reynolds numbers. This anomaly can be attributed to the program's difficulty in discerning between actual droplets and the other liquid formations in the spray. Otherwise, the size of the droplet decreases for each percentile with the increase in Reynolds number.

Table 2. Spray characteristics of TDA injector at 2 kV

Shadowgraphy	Re=780 We=110	Re=1090 We=210	Re=1550 We=440	Re=2190 We=860
Ø's Downstream	37	40.6	42.6	48.3
Particles	932	5151	5184	9518
D10 (mm)	0.246	0.171	0.108	0.098
D32 (mm)	0.413	0.352	0.227	0.225
DV10 (mm)	0.378	0.232	0.142	0.134
DV50 (mm)	0.629	0.660	0.360	0.374
DV90 (mm)	1.095	1.135	0.680	0.784

Similarly, the spray characteristics of the 3 kV time averaged images are displayed in Table 3. Upon inspection of the number of particles in each of the 3 kV sets it is apparent that the increase of voltage atomized more of the fuel. The number of particles at a Re=780 is 2098 while the same Reynolds number at 2 kV only produced less than half that number of droplets. However, the data does provide exceptions to the trend that larger applied voltages atomize more spray. The Re=2190 case has mean droplet

sizes and volume distributions that are slightly smaller than the same condition with the 2 kV spray.

As expected, the results with the TDA injector show that the spray break-up increased as the Reynolds number increased and as more voltage was applied across the electrodes of the injector despite differences in experimental setups and test conditions [1].

Table 3. Spray characteristics of TDA injector at 3 kV

Shadowgraphy	Re=780 We=110	Re=1090 We=210	Re=1550 We=440	Re=2190 We=860
Ø's Downstream	37	40.6	42.6	48.3
Particles	2098	3763	5753	11910
D10 (mm)	0.266	0.163	0.117	0.103
D32 (mm)	0.408	0.257	0.252	0.224
DV10 (mm)	0.386	0.201	0.155	0.142
DV50 (mm)	0.68	0.361	0.405	0.369
DV90 (mm)	0.976	0.563	0.799	0.605

Analysis of the USMA Injector

The experiments using the USMA injector produced results similar to those with the TDA injector. The rectangular geometry of the USMA nozzle enhanced the steadiness of the liquid stream, and removed issues with nozzle obscuration in the case with no applied voltage. Due to the different geometry, the Reynolds numbers were slightly different between the tests with the USMA injector when compared to the TDA injector when tested at the same pressures. For example, at 2 and 4 psi the TDA injector's spray had Reynolds numbers of 780 and 1090. At the same pressures the USMA nozzle produced Reynolds numbers of 960 and 1420, though the general trends remain unchanged.

Figure 18 indicates that the steady stream of the rectangular orifice was broken up with the application of 3 kV across the nozzle. As the Reynolds number increases, the droplet spacing decreases and there is evidence of lateral spreading of the droplets in the two higher Re cases.

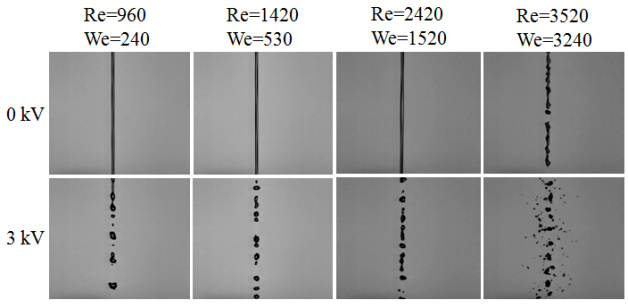

Figure 18. Array of USMA injector spray with and without electrical charge at increasing Reynolds numbers at 201 nozzles diameters below the exit plane.

In the analysis of the USMA injector, images were processed over 1.25 ms. Only one in every six of the 6000 images from each video were utilized to decrease volume of data. Figure 19 depicts the droplet distribution for flows with Reynolds numbers that range from 960 to 2420. Although there is a distinct difference in the spray distribution between the Reynolds numbers of 640 and 1610, the increase in atomization of the spray is more difficult to see compared to the TDA injector's distributions. However, the quantity of droplets at smaller diameters increases as the Reynolds number increases just as with the TDA nozzle.

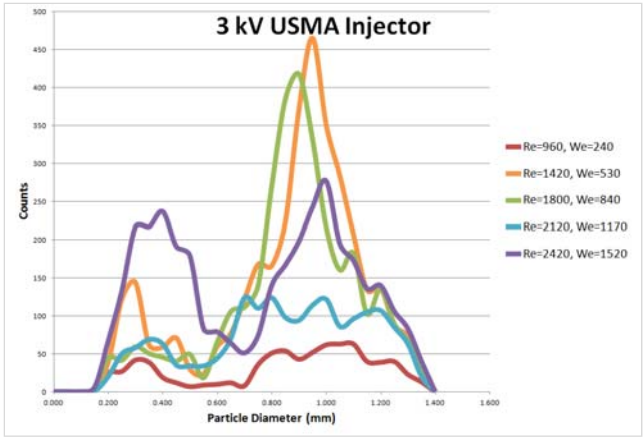

Figure 19. Droplet distributions by particle diameter for the 3 kV case and the USMA injector.

Spray characteristics for the USMA injector at 3 kV are presented in Table 4. The number of particles generally increases through the video sets, with one exception at a Reynolds number of 2120 despite a similar processing methodology. Generally, from left to right in the table the spray characteristics decrease as the Reynolds number is increased. The general behavior of the spray appears similar to the TDA Research nozzle case, though less pronounced and with more apparent deviations. As before, electric field and geometry conditions are expected to have a pronounced effect on the overall spray field and especially in the droplet statistics.

Table 4. Spray characteristics of USMA injector with 3 kV

Shadowgraphy	Re=960 We=240	Re=1420 We=530	Re=1800 We=840	Re=2120 We=1170	Re=2420 We=1520	Re=3520 We=3240
Ø's Downstream	201	201	201	201	201	201
Particles	856	3798	3436	1973	3748	11619
D10 (mm)	0.830	0.844	.851	0.823	0.74	0.431
D32 (mm)	1.020	0.979	.966	1.000	0.989	0.804
DV10 (mm)	0.890	0.890	0.854	0.824	0.871	0.495
DV50 (mm)	1.200	1.110	1.090	1.209	1.160	1.090
DV90 (mm)	1.430	1.390	1.396	1.425	1.421	1.399

Uncertainty

A number of uncertainties are associated with our measurement procedures. In order to assess the nozzle dimensions, we used the specified length and width in the EDM Labs order and used twice their reported tolerances as our uncertainty to account for the difficulty in producing sharp corners. This uncertainty has almost no effect on the other calculations. The flow was metered using a timer and graduated cylinder placed under the spray of the nozzle. The spray velocity was calculated from the volumetric flow rate and nozzle orifice area assuming a constant flow rate. Liquid fuel density was determined by using the same cylinder for volume and tare weight measurement.

Additional values such as the dynamic viscosity and surface tension of JP-8, which were used to calculate the Reynolds and Weber numbers, were obtained from the Handbook of Aviation Fuel Properties [15]. The relative uncertainties of these values were assumed to be about 5% in order to account for inconsistencies and variability in liquid properties. The purity of the fuel, changes in temperature, and evaporation all can change these characteristics.

The Kline-McClintock equation was used to calculate the uncertainty for the Reynolds number and Weber number calculations, each of which depended on the flow and fuel properties [19]. The Reynolds number uncertainties are recorded in Table 5, and the Weber number is reported in Table 6. Most of the uncertainty for the Weber number stems from uncertainty in the fluid velocity, but it is also significantly affected by the uncertainty associated with the surface tension, which can quickly change with the fuel temperature. The Reynolds number's uncertainty comes primarily from the uncertainty associated with the dynamic viscosity and secondarily from the velocity. While uncertainty values take into account the variation of fluid properties, flow uniformity, variation of liquid characteristics, and the similarity of the fuel to that described in the Handbook of Aviation Fuel Properties all affect the accuracy of the results [15].

Practical limitations of the LaVision DaVis software also contributed to uncertainty in the experiment. The software relies on intensity parameters to define the droplets. As such, there is a trade-off between particle recognition and noise. In the analysis region of the USMA injector, the fluid had elements of particles, ligaments, and amorphous blobs. Using a conservative definition for a particle, at any particular image assessed, the software did not take into account ligaments that would soon become particles. The prominence of ligament behavior in this region likely contributed to the inconsistencies in the analysis and droplet diameter distribution.

Conclusion

The objectives of this work were to assess the effects of electrostatic injection on the spray break-up process of JP-8 fuel. The approach to this objective included tests on an electrostatic injector developed by TDA Research Inc. as well as a rectangular nozzle incorporating a new electrostatic injector design.

Ultimately, the tests affirmed the results obtained by TDA Research. Increasing the electric field strength advanced the onset of atomization of the JP-8 spray. However, as the fuel pressure, and thus Reynolds number, is increased the electrostatic effects were dampened by surface tension. Finally, in TDA's fuel injector there was a cap that acted as the positively charged electrode and the nozzle itself acted as the negative secondary electrode. As a result, the electric field did not perpendicularly bisect the fuel flow.

Table 5. Reynolds numbers for the USMA injector with their associated relative uncertainties

PSI	Reynolds Number	Absolute Uncertainty
2	960	70
4	1420	94
5	1630	106
6	1800	115
8	2120	134
10	2420	151
15	3000	190
20	3520	221

Table 6. Weber numbers for the USMA Injector with their associated relative uncertainty

PSI	Weber Number	Absolute Uncertainty
2	240	24
4	530	40
5	700	48
6	840	55
8	1170	71
10	1520	87
15	1045	125
20	3240	166

Tests of a different design for the electrostatic injector established less pronounced effects when compared across the range of Reynolds and Weber numbers tested. However, rather than attempting to atomize a thin film from a flat fan nozzle the rectangular geometry also had a large volume of fuel being inject is due to the increased cross sectional area. It is reasonable to observe less pronounced

effects of the charge in the latter case because the surface tension of the stream is higher than for the thinner film. In either configuration, the break-up from a steady stream of fuel by applying charge across its electrodes was similarly enhanced.

Future work will include an experimental investigation into the electrostatic spraying of biofuels, particularly with application as fuel sources to power small unmanned aerial systems. Comparing the experimental results reported here and in future testing with simulation results will be another area of future research. Computational efforts will employ high-quality detailed numerical simulations of electrically charged sprays using techniques reported in the literature [16,17]. Using high-fidelity DNS techniques to simulate the near-nozzle region will elucidate the dominate break-up mechanisms in primary atomization and key features of atomization processes, such as the onset of atomization spray cone angle, Sauter mean diameter, drop size distributions, and ligament formation and orientation for comparison with the experimental results reported here. Additional simulations can be employed further downstream to model secondary atomization processes using advanced techniques, such as the one proposed by Herrmann [18] and modeling to account for evaporation.

Acknowledgments

The authors would like to express thanks to the technician team at the Vehicle Technology Directorate of the US Army Research Laboratory. Dr. Jim Nabity of the University of Colorado and Dr. Brad Spatafore of UC Boulder were immensely helpful in the recreation of their own experimental set-up. Special thanks also go to Mr. Jeff Butler of the Department of Civil and Mechanical Engineering, West Point, for his expertise in the machine shop during the fabrication process.

References

1. Nabity, J. A., Spatafore, B. M., Jenson, R., Daily, J. W., Van Poppel, B., Desjardins, O., O'Loughlin, C., and Hertzberg, J., 2012, *MEMS Pulsed Injection Electrostatic Atomizer for Small Engines*, Research Triangle Park, NC, TDA-1266-F
2. Van Poppel, B., 2010, *Numerical Methods for Simulating Multiphase Electrohydrodynamic Flows with Application to Liquid Fuel Injection,* Boulder, CO.
3. Rayleigh, L, 1882, "On the Equilibrium of Liquid Conducting Masses," *Philosophical Magazine Series 5*, 14:184-186.
4. Taylor, G.,1996, "Studies in Electrohydrodynamics. i. the Circulation Produced in a Drop by Electrical Field," *Proceedings of the Royal Society of London. Series A, Mathematical and Physical Sciences (1934-1990)* London, Great Britain.
5. Kim, K. and Turnbull, R., 1976, "Generation of charged drops on insulating liquids by electrostatic spraying," *Journal of Applied Physics*, 47(5).
6. Shrimpton, John, 2009, "Charge Injection Systems: Physical Principles, Experimental and Theoretical Work." *Heat and Mass Transfer*.
7. Shrimpton, J. and Yule, A. J., 1999, "Characterization of charged hydrocarbon sprays for application in combustion systems." *Experiments in Fluids* 26, no. 5, pp. 460-469.
8. Lehr, W. and Hiller, W., 1993, "Electrostatic Atomization of Liquid Hydrocarbons." *Journal of Electrostatics*, Vol. 30, pp. 433-440.
10. Shrimpton, J.S. and Yule, A.J., 1999, "Atomization, combustion, and control of charged hydrocarbon sprays," *Journal of Atomization and Sprays*, 11: 365-396.
11. Capecelatro, J., Owkes, M., and Desjardins, O., 2014, *Using Supercomputers to Study Biofuel Production and Injection*, Presentation to Department of Civil and Mechanical Engineering. West Point, NY.
12. Gibson, T'Jae, 2012, "ARL's combustion lab sparks studies that could lead to JP-8 'super engine'" Aberdeen Proving Ground, MD, http//www.army.mil.
13. Turbine Fuel, Aviation, Kerosene Type, JP-8 (NATO F-34), NATO F-35, and HP-8+100 (NATO F-37) MIL-DTL-83133H w/ AMENDMENT 1
14. Callister, Jr., W. D., and Rethwisch, D. G., 2010, *Material Science and Engineering: An Introduction*, John Wiley and Sons, Inc., New York.
15. Propulsion Directorate, Air Force Material Command, 2004, *Coordinating Support of Fuels and Lubricant Research and Development*, Coordinating Research Council, Alpharetta, GA.
16. Van Poppel, B.P., O. Desjardins, and J.W. Daily. 2010. "A Ghost Fluid, Level Set Methodology for Simulating Multiphase Electrohydrodynamic Flows with Application to Liquid Fuel Injection." Journal of Computational Physics 229: 7977–7996.
17. Owkes, M., Desjardins, O., "Consistent and conservative computational framework for simulations of electrohydrodynamic (EHD) atomization", ILASS Americas 26th Annual Conference, Portland, OR, May 2014
18. Herrmann, M. 2010. "A Parallel Eulerian Interface Tracking /Lagrangian Point Particle Multi-Scale Coupling Procedure." Journal of Computational Physics 229 (3): 745–759.
19. Kline, S. J., and F. A. McClintock. "Describing Uncertainties in Single-Sample Experiments." Mechanical Engineering, Vol. 75, No. 1, January 1953: 3-8.

1 (PDF)	DEFENSE TECHNICAL INFORMATION CTR DTIC OCA
2 (PDF)	DIRECTOR US ARMY RESEARCH LAB RDRL CIO LL IMAL HRA MAIL & RECORDS MGMT
1 (PDF)	GOVT PRINTG OFC A MALHOTRA
6 (PDF)	DIR USARL RDRL VTP L BRAVO M KURMAN C-B KWEON S MINTZ M SZEDLMAYER M TESS
7 (PDF)	US MILITARY ACADEMY DEPT OF CIVIL & MECHL ENGRNG M BENSON D EICHNER Z LEE M RYAN T SOWELL J TENNIS B VAN POPPEL